Integrated CMOS Receiver for Wearable Coil Arrays in MRI Applications

Benjamin Sporrer†, Luca Bettini†, Christian Vogt*, Andreas Mehmann*, Jonas Reber‡, Josip Marjanovic‡, David O. Brunner‡, Thomas Burger†, Klaas P. Pruessmann‡, Gerhard Tröster* and Qiuting Huang†
†Integrated Systems Laboratory, ETH Zurich, Zurich CH-8092, Switzerland
*Electronics Laboratory, ETH Zurich, Zurich CH-8092, Switzerland
‡Institute for Biomedical Engineering, ETH Zurich and University of Zurich, Zurich CH-8092, Switzerland
Email: sporrerb@iis.ee.ethz.ch

***Abstract*—Surface coil arrays brought in proximity of the human body enhance the performance of an MRI measurement both in speed and signal-to-noise ratio. However, size and cabling of such arrays can deteriorate the performance of the imaging, or put at risk the safety of the patient. An integrated CMOS direct conversion receiver is proposed, to be placed directly onto the receive coil and enhance the usability. The integrated design needs to preserve the high performance (both in silent noise figure and dynamic range) of discrete solutions, which benefit from dedicated technologies for every receiver sub-block. To exploit the full potential of a coil array, the receiver on each module must also minimize the coupling to nearby modules. The PCB carrying the ASIC will be fabricated with flexible substrate materials to further enhance the wearability and comfort for the patient. Such a modular approach together with the transmission of data over optical fibers results in a lightweight system that allows us to achieve fast development times.**

I. Introduction

Magnetic Resonance Imaging (MRI) is one of the most widely used imaging techniques in medical diagnostics. A great variety of anatomical and functional features, processes, and diseases can be visualized with this approach. MRI relies on the combined effects of three types of magnetic fields. A powerful superconducting magnet generates a uniform, static background field, which causes a split in the spin states of hydrogen nuclei in the body. Radio-frequency (RF) excitation fields with amplitudes in the μT range are used to induce transitions and coherence between the two resulting states. The coherence gives then rise to resonance signals at the same frequency, with powers in the pW to nW range. Finally, intricate choreographies of audio-frequency gradient fields in the range of several mT are used to modulate the resonance frequency for image encoding. Image reconstruction is then achieved by signal processing of the data acquired through RF receive coils placed near the target anatomy.

Volume (e.g. birdcage) [1] and surface coils [2] are the two main types of RF coils employed in MRI applications [3]. The former benefits from a highly homogeneous magnetic field. Birdcage detectors are rigid, which compromises the comfort for the patient. In addition, mechanical rigidity does not permit to adjust the detector to the actual size and shape of the target anatomy degrading sensitivity, also preventing changes in posture, such as the flexion of the joint. In an MR system, the spatial encoding of the image is obtained by frequency and phase encoding with the help of gradient fields superimposed on the static magnetic field of the MRI bore. The maximum gradient strength and slew rate that can be created by the gradient coils limit the image encoding, and, therefore, the maximum speed at which the image can be acquired. This problem is very similar to the bandwidth limitation experienced in a modern cellular communication receiver. Multiple-input multiple-output (MIMO) represents a common approach to tackle bandwidth limitation in a wireless receiver, which has been pioneered by [4] in the early nineties. The resolution of a transmitted signal is improved in time and amplitude by receiving it over several channels with ideally linearly independent responses. The same principle has been proposed for MR measurements in [5]. Several surface coils are placed at different positions near the imaging volume. Such coils have different sensitivity distributions on the image, which correspond to the individual channel responses in MIMO systems. Without increasing the gradient performance, the speed of the imaging and the SNR of the acquired image (i.e. sensitivity) can be therefore increased.

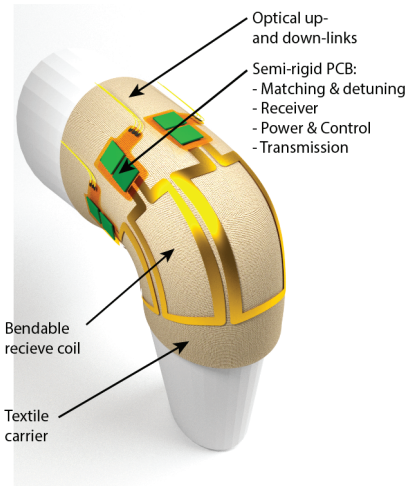

Fig. 1. Prototype of the wearable coil array and integrated electronics.

Multi-channel data acquisition with RF detector arrays represents nowadays the most effective way to mitigate the sensitivity and speed limits of MRI measurements [6], [7]. The optimal sensitivity is achieved when a large number of small surface coils closely fits the target anatomy [3]. This

978-3-9815370-4-8/DATE15/©2015 EDAA

results in a high signal-to-noise-ratio SNR, and a high spatial encoding. The main drawback of scaling up multi-channel coil arrays to several tens of acquisition channels is the need for a large number of shielded RF cables to transmit the analog information out of the magnetic field. Systems deploying up to 128 acquisition channels have been demonstrated [8]. In order to ensure safety for the patient, a huge infrastructure effort has to be spent in the cables installation. They have to be guided mechanically, and they have to be equipped with baluns and cable traps. Currents on the shields, grounding, parasitic coupling between coaxial cables can in fact severely degrade the signal integrity, and therefore the sensitivity. Moreover, the stiffness of the cables affects the ease of use and the comfort for the patient. Finally, shielded RF cables are expensive and, when several tens of channels are employed, can have a significant impact on the budget of the entire MRI system.

A valid alternative to avoid a large number of coaxial cables is to replace them with optical glass fibers. An analog optical link has already been demonstrated [9]. Coupling analog signals to an optical fiber can compromise the noise figure (NF), but alleviates the requirements on the receiver side. On the other hand, a digital optical link does not affect the linearity or the NF, simplifying the design of the optical link itself, but requires digitization directly in-bore. For these reasons, the integration of the RF receiver in a modern CMOS technology is the key enabler that allows us to shrink the size of the receivers and place them on the receive coils, performing the digitization of the acquired data directly in-bore. This enables the use of optical fibers for data transmission, avoiding coaxial cables with significant benefits from the cost and the usability point of view.

In this contribution, we present the design of wearable, adaptive detector arrays for 3 T and 7 T MRI measurements, equipped with fully integrated CMOS receivers for in-bore digitization (Fig. 1). The MRI receiver application-specific integrated circuit (ASIC) deploys direct conversion rather than direct sampling, in order to save power, and alleviate the requirements of the A/D conversion. The remaining of the paper is organized as follows. Section II describes the wearable MRI module. Section III provides system level considerations for the receiver integration. Section IV presents the receiver design, and finally, conclusions are drawn in Section V.

II. Wearable MRI module

The array coils are fabricated on a flexible substrate coated with 14µm of copper. A stand alone semi-rigid wearable MRI receiver printed circuit board (PCB) is constructed (Fig. 2 and Fig. 3) for each receive module. Each PCB hosts the RF chain, digitization and data transmission of the sampled signal outside of the magnetic field. It needs to comply with stringent electromagnetic compatibility (EMC) criteria, such as $200\,\mathrm{T\,m^{-1}\,s^{-1}}$ magnetic field alternation and RF pulses of several tens of kilowatts in the range between 128MHz to 298MHz, which are generated during the MRI scanner operation [10]. In order to comply with these requirements, the PCB layout is rigorously optimized with the help of finite element method (FEM) simulations to improve EMC robustness. Care must be taken to the magnetism of the components to prevent the introduction of any disturbances into the magnetic field near the receiver coils. Furthermore, fiber optical links are used to control the receiver and transmit the digitized data outside of the magnetic field for subsequent image reconstruction.

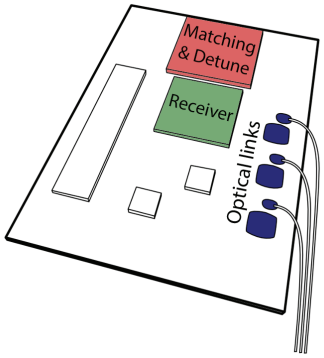

Fig. 2. Semi rigid PCB including receiver, optical communication and control.

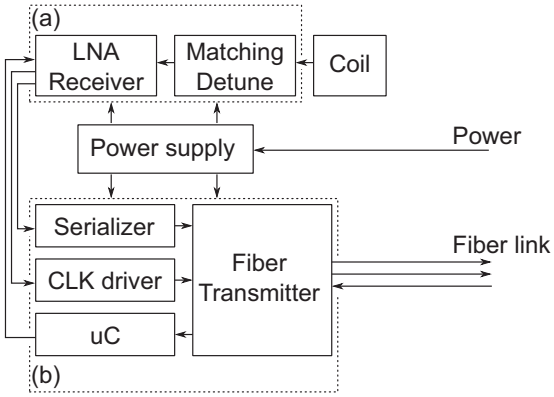

Fig. 3. Schematic overview of wearable MRI electronics for a single coil receiver. The RF modules are shown in (a), the digital module in (b).

The RF chain on each wearable MRI module consists of the matching and detune network to protect the electronics during the proton excitation RF pulse, as well as the low noise amplifier (LNA) and integrated receiver, as shown in Fig. 3(a). Both blocks are set up as exchangeable rigid PCBs to provide sufficient mechanical stability and a low loss dielectric. Additionally, this setup allows an easy exchange of the matching network depending on the coil geometry used.

The digital part of the design in Fig. 3(b) is based on a flexible PCB substrate. This allows us to fold the digital electronic on top of the rigid RF modules. The digital part consists of a glass fiber up-link processed by a micro-controller to initialize and adjust the integrated receiver and LNA settings, as well as a serializer used for the data down-link. This serializer is used to convert the parallel data output of the integrated receiver into a serial stream to be transmitted over the glass fiber link.

The clock on the module needs to be phase locked to the main system clock to allow proper image reconstruction. One possible implementation of the phase lock is to send the MRI system clock via an optical up-link to the receiver module, as shown in Fig. 4(a). The drawback of this approach is the substantial phase noise added by the optical link. A narrow-band PLL with a loop-bandwidth in the sub-kHz range needs

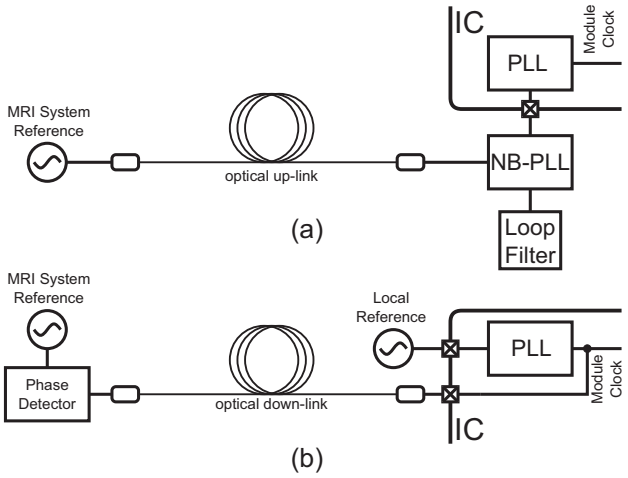

Fig. 4. Methods to achieve phase lock between the module clock and the MRI system reference with a centralized topology with narrow-band PLL (NB-PLL) (a) or a distributed topology with local reference (b).

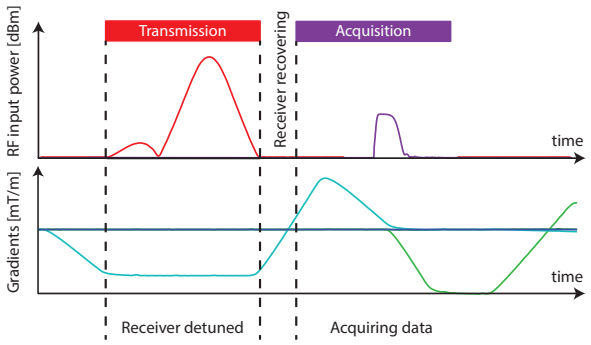

Fig. 5. Sketch of the input signal power and gradient switching during a single measurement.

to be placed on the PCB to filter the additional noise of the link. To minimize the component count on the receiver module, a distributed approach has been adopted and is depicted in Fig. 4(b). The clock is generated locally by a free running oscillator, and the integrated PLL synthesizes the required clock frequencies from this oscillator. The synthesized clock is then sent outside the magnetic field via optical down-link. There the free running module clock is compared to the MRI system clock by means of a low noise phase detector. The information on the phase error from the phase detector can then be used to cancel the error in the digital post processing.

Power is supplied to the wearable MRI module over copper cables with additional RF filtering. This power supply is afterwards distributed to the digital and RF modules, which deploy individual linear voltage regulators to stabilize each supply voltage and reduce coupled RF noise on the power supply. DC/DC converters are not used in this design because either they require large inductances or capacitances that are not commercially available as non-magnetic components or their switching frequency is high enough that its harmonics may disturb the reception.

III. Receiver Planning

The carrier frequency of an MRI signal depends on the strength of the main constant field of the system and on the type of nuclei to be imaged. In most cases protons are to be imaged, which have a resonance frequency at $f_r = 42.58\,\mathrm{MHz/T} \cdot B_0$. This results in RF carrier frequencies of 128 MHz and 298 MHz respectively for the common 3 T and 7 T MRI systems. By applying gradient fields, the local magnetic field strength is made dependent on the position within the volume. The resonance frequency is therefore spatially encoded allowing the reconstruction of the imaging volume. The bandwidth of the RF signal produced by the spreading of the resonance frequency can be as large as 1 MHz [11].

A typical input signal that reaches the MRI receiver is depicted in Fig. 5. The tissue under examination gets excited by a very strong RF pulse at the carrier frequency. During this time, the receiver has to be protected from the large incoming signals that otherwise would overload or destroy the receiver circuitry. The resonance frequency of the coil has to be shifted away from the proton resonance frequency to ensure the coil is not disturbing the spatial homogenity of the RF excitation pulse or even generating a safety risk for the nearby patient. For this reason, the coil is detuned and the currents on it are blocked by a diode-switching trapping circuit. After the RF excitation pulse is turned off, an exponentially decaying response signal from the tissue can be captured. The receiver has to recover from the protected detune state within a few microseconds to ensure optimal signal yield. After the signal has decayed, the pulse and acquisition scheme is repeated until the whole image is captured.

A. Receiver Topology

Two major approaches used in MRI receivers can be distinguished, the direct-sampling receiver and the direct-conversion/low-IF receiver as shown in Fig. 5. In the former case, the signal is amplified, filtered and finally sampled exclusively at the RF carrier frequency. The signal is sub-sampled to alleviate the requirements on the analog-to-digital converter (ADC). The sampling frequency of the ADC is therefore placed well below the Nyquist rate for the input signal [12]. A band-pass shaped anti-aliasing filter centered around the RF signal frequency has to be placed in front of the ADC to prevent folding of other noise bands into the ADC signal band. The direct sampling topology is well suited for discrete receivers because only a small number of components is needed. On the PCB, the anti-aliasing can be realized with an LC filter with sufficient quality factor or for certain frequencies with compact surface acoustic wave (SAW) filters, whereas in an integrated implementation this would result in a very bulky design.

On the other hand, low-IF or direct conversion receivers are much more amenable to integration. They translate the carrier frequency down to low or zero frequency, respectively. Quadrature mixers are used to reject the noise at image frequencies. Quadrature mixers and their driving circuitry are area consuming and susceptible to interference when implemented with discrete components, and their complexity is more suited for an integrated solution. After down-conversion, the signal is amplified at frequencies below 1 MHz in the case of direct conversion. This allows one to employ feedback

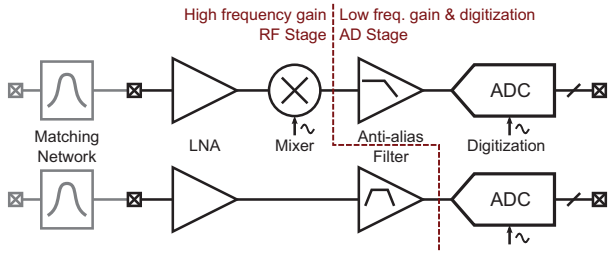

Fig. 6. Block diagram of direct conversion (top) and direct sampling (bottom) architectures.

structures in the following amplifiers to improve linearity. In such topologies, the ADC sampling rate will be above the Nyquist rate, therefore low-pass filters are sufficient to perform the anti-aliasing operation. Mitigating gain stages and filtering to much lower frequencies, replacing band-pass with simple low-pass filters and reducing the ADC sampling rate all reduce the power consumption of this approach compared to the direct sampling. Changing the carrier frequency requires only a change in the local-oscillator (LO) clock frequency, which can be realized by a programmable frequency synthesizer on the IC. In the direct sampling topology, the center frequency of the anti-alias filter needs to be changed, which is more challenging.

B. Noise Figure & Dynamic Range

The two most important figures of merit for an MRI receiver are the noise figure and the dynamic range (DR). Degrading the noise figure of an MRI receive chain directly translates into an increased scan time (i.e. for an increase in noise figure of 3 dB the scan time has to be doubled). Silent noise figures $\mathrm{NF}_{\mathrm{tot},0}$ of receivers with discrete implementation range between 1 and 2 dB [3].

The SNR of the incoming MRI signal decays over time. The peak input power at the beginning of a measurement strongly varies with size, shape and position of the receive coil, and it can exceed -40 dBm. Considering a signal bandwidth of 1 MHz, this translates into a peak source SNR of 74 dB and higher. Besides having a low $\mathrm{NF}_{\mathrm{tot},0}$, the receiver must be linear enough to convey also these high signal levels without adding noticeable distortions. In both topologies, the distortion is mainly generated by third order non-linearities. In the baseband and conversion stages also second order harmonics can fall into the signal band at certain input frequencies. This can usually be avoided by a proper choice of the down-conversion or ADC clock frequency, respectively. Fig. 7 shows the trade-off between the noise figure of the RF and AD stages (as shown in Fig. 6) and the third order intermodulation distortion (IM3) of the receive chain at a source SNR of 74 dB with a budget of 3 dB for receiver added noise and distortion (i.e. the output signal-to-noise-and-distortion-ratio $\mathrm{SNDR}_{\mathrm{out}} = \mathrm{P}_{\mathrm{sig,out}} / \left(\mathrm{N}_{\mathrm{tot,out}} + \mathrm{P}_{\mathrm{dist,out}}\right)$ equals 71 dB). Increasing the gain in front of or within the AD stage usually leads to a lower silent noise figure $\mathrm{NF}_{\mathrm{tot},0}$, but it severely decreases $\mathrm{SNDR}_{\mathrm{out}}$. The gains of the different stages have to be planned very carefully to maximize $\mathrm{SNDR}_{\mathrm{out}}$ and/or minimize $\mathrm{NF}_{\mathrm{tot},0}$. Variable gain structures offer the possibility to optimize the gain planning for different coil array setups by configuring the receiver ASIC.

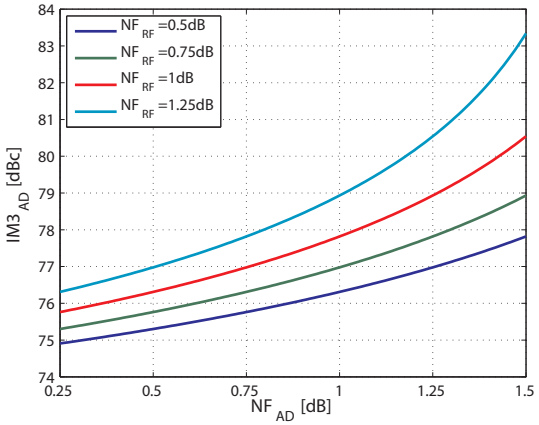

Fig. 7. Required linearity (total inband IM3) of the AD stage as a function of the noise figures from the RF and AD stages for a source SNR of 74 dB and an output SNDR of 71 dB.

C. Receiver Input Matching

In a surface coil array, many receive coils are placed next to each other. This means that a significant mutual induction occurs between different receiver coils. To prevent coupling between the receive channels, the LNA input is chosen to be reflective, i.e. the matching networks output impedance $\mathrm{Z}_{\mathrm{MN,out}}$ and the input impedance of the LNA $\mathrm{Z}_{\mathrm{LNA,in}}$ are chosen such that Γ_{LNA} assumes an absolute value near to 1, where

$$\Gamma_{\mathrm{LNA}} = \frac{\mathrm{Z}_{\mathrm{LNA,in}} - \mathrm{Z}_{\mathrm{MN,out}}}{\mathrm{Z}_{\mathrm{LNA,in}} + \mathrm{Z}_{\mathrm{MN,out}}}.$$

This is achieved by choosing the real parts of the impedances according to $\mathrm{Re}\left(\mathrm{Z}_{\mathrm{LNA,in}}\right) \gg \mathrm{Re}\left(\mathrm{Z}_{\mathrm{MN,out}}\right)$ or $\mathrm{Re}\left(\mathrm{Z}_{\mathrm{LNA,in}}\right) \ll \mathrm{Re}\left(\mathrm{Z}_{\mathrm{MN,out}}\right)$. The matching network converts this impedance mismatch into a very high series resistance at the receive coil, suppressing the current from flowing at the receive frequency and therefore minimizing any inductive coupling to neighboring coils. To minimize the noise figure, the noise match impedance of the LNA $\mathrm{Z}_{\mathrm{LNA,opt}}$ must be equal to $\mathrm{Z}_{\mathrm{MN,out}}$. The LNA must therefore have a $\mathrm{Z}_{\mathrm{LNA,opt}}$ with either a much higher or much lower real part than $\mathrm{Z}_{\mathrm{LNA,in}}$ to minimize coupling between coils and show an optimal noise figure.

D. Distortion

By placing a receiver inside the in-bore field, the circuit is exposed to the strong magnetic fields mainly due to the gradient coils. The gradient fields are generated at acoustic frequencies far lower than the RF receive signals at more than 100 MHz. Nevertheless, nonidealities in the circuit can modulate the distortions into the signal band. Furthermore, distortions on the supply rails can also appear in the final output signal. Coupling to nodes within the PLLs generating the local clock signals can lead to modulation of their output frequencies. The time-dependent magnetic flux through a loop formed by a signal and its return current path with an area A induces a voltage

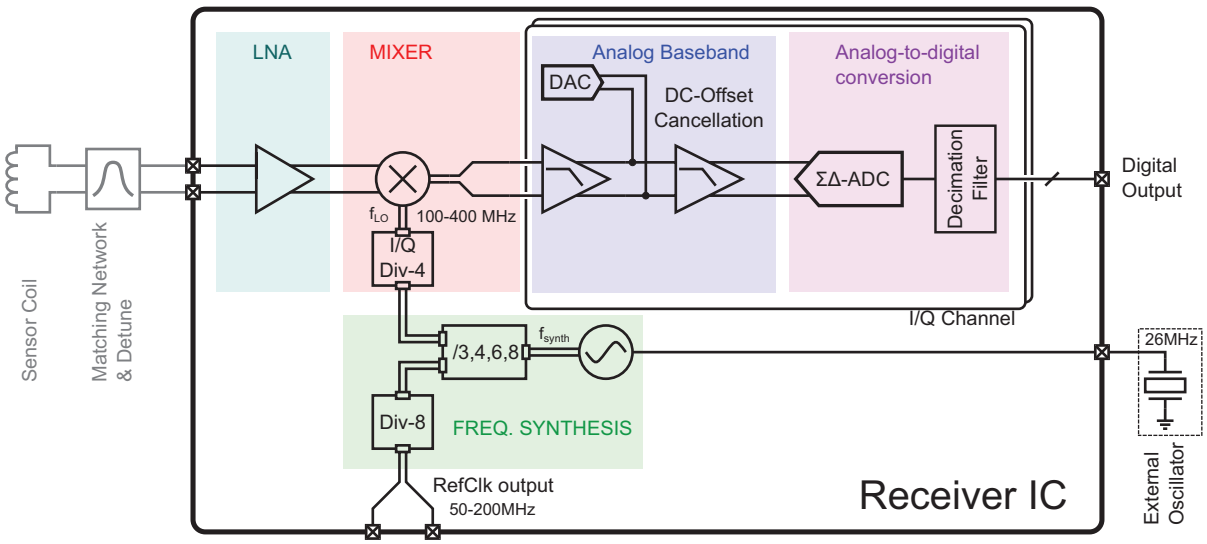

Fig. 8. Blockdiagram of the direct conversion receiver IC. All baseband components are instantiated once for I and Q channels.

$$V_{\text{ind}} = \frac{d\Phi}{dt} = \vec{A}\frac{d\vec{B}_0(t)}{dt}$$

on this loop, where $\frac{d\vec{B}_0(t)}{dt}$ (up to $200\,\mathrm{T\,s^{-1}}$ in absolute value) is the variation in the magnetic field density produced by the gradient coils of the MRI system. Signal connections between discrete components on PCB reach a length of several millimeters. Assuming a trace length of $1\,\mathrm{cm}$, $1\,\mathrm{mm}$ distance from the trace to the return current path and the magnetic field being perpendicular to this loop, a voltage of $1\,\mathrm{cm}\cdot 1\,\mathrm{mm}\cdot 200\,\mathrm{Ts^{-1}} = 2\,\mathrm{mV}$ is induced on the loop. For an integrated circuit the distances in signal paths are much shorter, a trace length of $1\,\mathrm{mm}$ and a return path distance of $50\,\mu\mathrm{m}$ are reasonable assumptions. Thus, the induced voltage on the integrated signal path results in $1\,\mathrm{mm}\cdot 50\,\mu\mathrm{m}\cdot 200\,\mathrm{Ts^{-1}} = 10\,\mu\mathrm{V}$, which makes integrated signal paths much less susceptible to the magnetic interference.

Decoupling a supply rail against frequencies in the acoustic range requires large elements being placed on the PCB, a small form factor and a low number of components is also in this case beneficial. In particular, distortions can be further tackled with circuit methodologies, e.g. deploying a fully differential design. Any disturbance on the supply or on the ground manifests itself as a common mode signal and gets rejected by fully differential stages. The receiver module also causes distortions to the gradient field used for spatial encoding, which undergoes nonlinear misshaping near metallic objects, and even more near magnetic materials as described before. Loops or planes of metal cannot be avoided but can be reduced by increasing the degree of integration.

E. Clock Jitter

At very high input SNR, the timing jitter of the module clock modulated onto the wanted signal by the mixer or by the sampling process inside the ADC can deteriorate the noise figure. The jitter is generated mainly by the output phase noise of the frequency synthesizer i.e. the integrated PLL. The timing jitter has a certain power spectral density $T_{\mathrm{j}}(j\cdot 2\pi f)$. We assume the timing jitter is modulated onto a sinusoidal input signal in the middle of the signal bandwidth. Only the jitter components below a frequency of $f_{\mathrm{BW}}/2$ and above a frequency $1/\mathrm{T}_{\mathrm{measurement}}$ are present in the signal bandwidth, therefore we define the rms time jitter as

$$t^2_{\mathrm{j,rms}} = \frac{1}{2\pi}\int_{1/\mathrm{T}_{\mathrm{measurement}}}^{f_{BW}/2} T_j^2(j\cdot 2\pi f)\mathrm{d}f.$$

It has been shown in [12] that even in-band rms jitter of only 300 fs can be the dominant noise source in an MRI receiver for a high source SNR.

IV. Integrated Receiver Design

The block diagram of the integrated receiver is shown in Fig. 8. It deploys the direct-conversion/low-IF architecture discussed in the previous section. The design comprises flexible frequency selection, power and area efficient low-pass filtering and a highly-linear ADC based on $\Delta\Sigma$-modulation. All stages of the receiver are fully differential. Therefore, this integrated solution does not contain any stage driven by single-ended signals as opposed to discrete component solutions, that need to minimize the transistor count and only have access to off-the-shelf components, which are often not available with differential inputs and outputs. As discussed in the previous section, this reduces the influence of all distortions coupling to the receiver.

In the LNA, shown in Fig. 9, the signal first passes through a main amplification stage. A feedback amplifier with a purely capacitive load at the RF frequencies of interest feeds an in-phase current back to the input through a capacitive feedback. This type of feedback used in a single-ended MRI LNA is proposed in [13]. The input resistance shown by this feedback approach is

$$\mathrm{R}_{\mathrm{LNA,in}} \approx \frac{1}{\mathrm{A}_{\mathrm{main}}\cdot\mathrm{G}_{\mathrm{m,fb}}}\cdot\frac{\mathrm{C}_{\mathrm{fb}}+2\mathrm{C}_{\mathrm{L}}}{\mathrm{C}_{\mathrm{fb}}} \quad \text{if} \quad \left|\frac{\mathrm{G}_{\mathrm{m,fb}}\mathrm{A}}{2\omega\mathrm{C}_{\mathrm{L}}}\right| \gg 1.$$

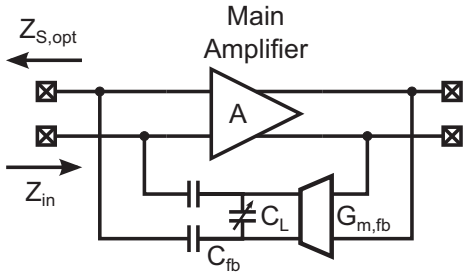

Fig. 9. Integrated LNA with capacitive feedback [13].

The mixer uses a divided version of the internal high frequency LC-tank based synthesizer as local oscillator. The oscillation frequency f_{synth} between 3.4 and 5.2 GHz is divided with a selectable ratio to the desired LO frequency. In the proposed direct conversion architecture, the LO frequency f_{LO} must be the same as the signal carrier frequency (i.e. either 128 MHz or 298 MHz). The selectable division ratio allows us to use different values of f_{synth} to produce the same f_{LO} as shown in Fig. 8. In this way, the region of optimal synthesizer phase noise can be identified. The output of the mixer is connected to the baseband filter stages providing the anti-alias filter to minimize noise for the following ADC stage.

Gain settings of the different stages of the receiver can be selected out of $A_{LNA} = 32...40dB$ and $A_{BB} = -12...19dB$, allowing a selectable receiver gain of $A_{tot} = 20...59dB$. To guarantee a low noise figure the gain before reaching the mixer should not be too low, making the design of the LNA more complex and possibly requiring a multi stage approach. The full range signal for the ADC is 0 dBm, allowing a maximum input power at the coil of -20 dBm.

V. Conclusion & Outlook

This work presents the system level design of a fully integrated on-coil receiver to be placed inside a wearable coil array within a common 3 T or 7 T MRI system. Such a compact system, featuring down-conversion and digitization, enables the optical transmission of the data to the signal processors located outside the magnetic field. The flexible wearable coil, together with the thin and bendable cabling, enables the fast assembly of surface coil arrays for dedicated purposes. The integration approach offers fully differential signaling and low coupling of e.g. gradient fields to the circuit because of substantial area reduction. Furthermore by using a standard CMOS process, one can efficiently integrate RF circuits, baseband stages and digital blocks on the same IC. This offers a very high flexibility and programmability of all elements of the receive chain.

Further steps in this ongoing project will be the introduction of an optical power transmission, and the receiver optimization to enable applications like field probing (as shown in [14]) of the in-bore magnetic field to further enhance image quality.

Acknowledgment

This research is funded by the Swiss Nano-Tera project WearableMRI.

References

[1] C. E. Hayes, W. A. Edelstein, J. F. Schenck *et al.*, "An efficient, highly homogeneous radiofrequency coil for whole-body NMR imaging at 1.5 T," *J Magn Reson*, vol. 63, pp. 622–628, 1985.

[2] E. B. Boskamp, "A new revolution in surface coil technology: the array surface coil," in *Proceedings of the 6th annual meeting of ISMRM*, 1987, p. 405.

[3] N. A. Massner, N. De Zanche, and K. P. Pruessmann, "Mechanically adjustable coil array for wrist MRI," *Magnetic Resonance in Medicine*, vol. 61, pp. 429–438, 2008.

[4] B. Ottersten and H. R. Richard, "Spatial division multiple access wireless communication systems," *U.S. Patent No. 5,515,378*, May 1996.

[5] P. B. Roemer, E. W. A., C. E. Hayes *et al.*, "The NMR phased array," *Magnetic resonance in medicine*, vol. 16, pp. 192–225, Jul. 1990.

[6] K. Pruessmann, M. Weiger, M. Scheidegger *et al.*, "SENSE: Sensitivity encoding for fast MRI," *Magnetic Resonance in Medicine*, vol. 42, pp. 952–962, 1999.

[7] M. Griswold, P. M. Jakob, R. M. Heidemann *et al.*, "Generalized autocalibrating partially parallel acquisitions (GRAPPA)," *Magnetic resonance in medicine*, vol. 47, p. 12021210, 2002.

[8] B. Stoeckel, A. Potthast, N. Oesingmann *et al.*, "An MRI system with 128 seamlessly integrated receive channels for multi-nuclear operation," in *Proc. Intl. Soc. Mag. Reson. Med.*, vol. 16, 2008, p. 1119.

[9] J. Yuan, J. Wei, and G. Yen, "A 4-channel coil array interconnection by analog direct modulation optical link for 1.5-T," *IEEE Trans. Med. Imag.*, vol. 27, pp. 1432–1438, Oct. 2008.

[10] M. A. Brown and R. C. Semelka, *MRI: Basic Principles and Applications*, 4th ed. John Wiley and Sons, 2011.

[11] Z.-P. Liang and P. C. Lauterbur, *Principles of magnetic resonance imaging*. IEEE Press, Series in Biomedical engineering, 2000.

[12] J. Reber, J. Marjanovic, D. Brunner *et al.*, "In-bore broadband array receivers with optical transmission," in *Proc. Intl. Soc. Mag. Reson. Med.*, vol. 22, Oct. 2014, p. 619.

[13] R. Oppelt and M. Vester, "A low input impedance MRI preamplifier using a purely capacitive feedback network," in *Proc. Intl. Soc. Mag. Reson. Med.*, vol. 14, 2006, p. 2026.

[14] N. De Zanche, C. Barmet, D. Meier, and K. P. Pruessmann, "NMR probes for magnetic field monitoring during MRI," in *Proc. Intl. Soc. Mag. Reson. Med.*, vol. 13, 2005, p. 791.